Supplementary Material for

First-principles study of the structural, electronic and elastic properties of FeO$_2$-

FeO$_2$He system under high pressure

Haibo Liu [a, *], Lei Liu [b, *], Cunlin Xin [c], Longxing Yang [d], Xiaoyu Gu [b]

[a] Key Laboratory of Geoscience Big Data and Deep Resource of Zhejiang Province, School of Earth Sciences, Zhejiang University, Hangzhou 310027, China

[b] United Laboratory of High-Pressure Physics and Earthquake Science, Institute of Earthquake Forecasting, China Earthquake Administration, Beijing 100036, China

[c] College of Geography and Environmental Science, Northwest Normal University, Lanzhou 730070, China

[d] State Key Laboratory of Geological Processes and Mineral Resources, School of Earth Sciences and Resources, China University of Geosciences, Beijing 100083, China

[*] Corresponding author: haibo@zju.edu.cn (H. Liu); liulei@ief.ac.cn (L. Liu)

This Supplementary Material includes:

Table S1

Figures S1 to S12

References

Table S1. Comparison of the results of FeO_2 and FeO_2He in this study with previous results.

					FeO$_2$					
P (GPa)	T (K)	a (Å)	V (Å³)	ρ (g/cm³)	<Fe-O> (Å)	<O-O> (Å)	O-Fe-O (°)	Fe-O-O (°)	Method	Reference
76		4.363	83.04	7.026					Exp	
76		4.331	81.23						Sim	Hu et al., 2016
76	273				1.792	1.937	95.6	99.1	Exp	
76	0				1.781	2.077	96.52	96.28	Sim	
76					1.808	1.896	95.26	99.92	Exp	Hu et al., 2016 Jang et al., 2017
76		4.364	83.115						Exp	Lu et al., 2018
76		4.364	83.104		1.787	2.232			Sim	Lu et al., 2018
76	0	4.364	83.105	7.021	1.794	2.104	96.581	96.659	Sim	this study
Δ (%)		0~0.76	0~2.31	0.07	0.11~0.77	1.30~10.97	0.06~1.39	0.39~3.26		
119			76.21		1.75	1.99			Sim	Shorikov et al., 2018
119	0		76.678		1.755	1.995			Sim	this study
Δ (%)			0.61		0.29	0.25				

			FeO$_2$He				
P (GPa)	T (K)	a (Å)	<Fe-O> (Å)	O-Fe-O (°)	Fe-O-Fe (°)	Method	Reference
135	0	4.32	1.87	70.53	109.47	Sim	Zhang et al., 2018
135	0	4.32	1.87	70.53	109.47	Sim	this study
Δ (%)	0	0	0	0	0		

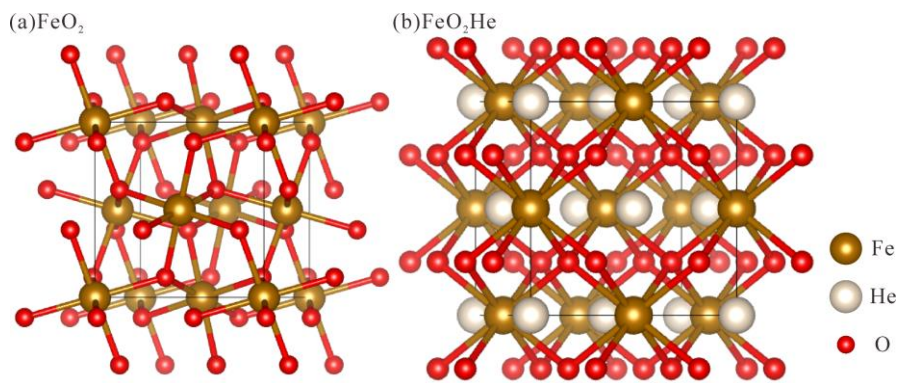Exp = Experiment; Sim = Simulation.

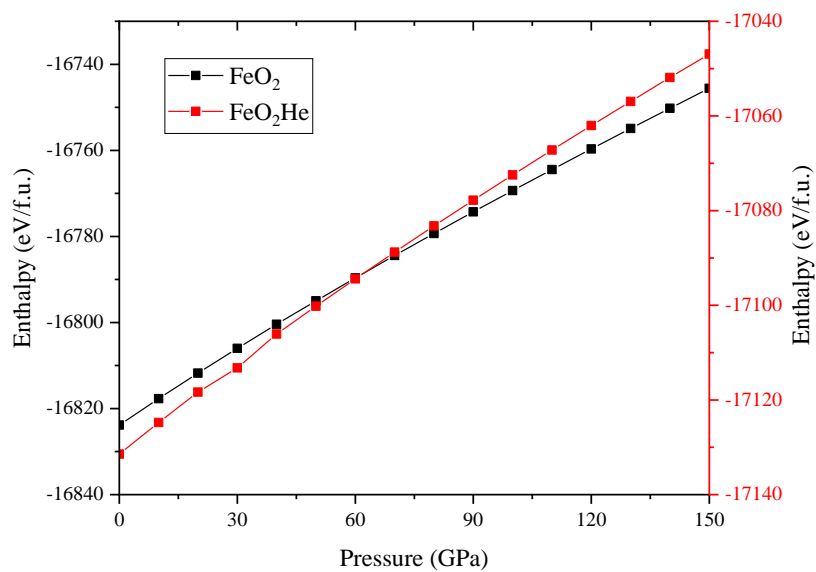**Fig. S1.** Crystal structures of (a) FeO_2 and (b) FeO_2He.

Fig. S2. Enthalpy of FeO_2 and FeO_2He at different pressures.
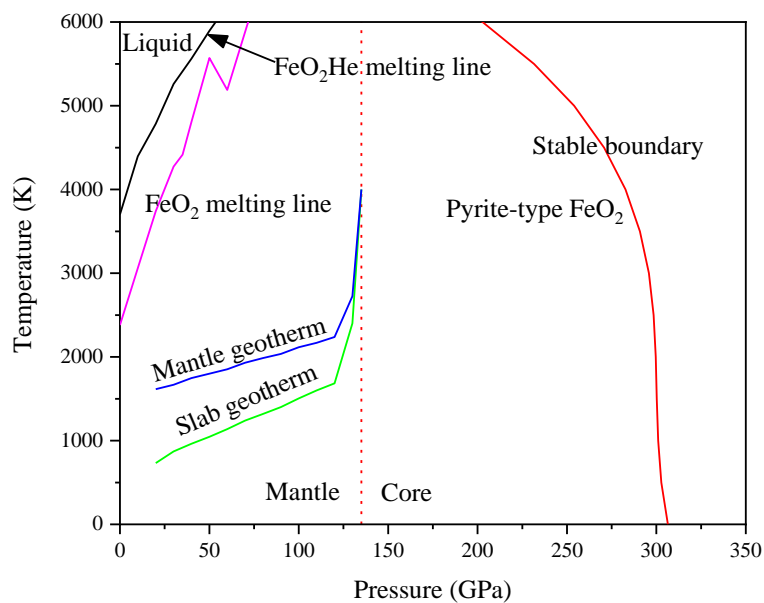

Fig. S3. Phase diagram of FeO_2 and FeO_2He at high temperature and high pressure. The

melting line of FeO$_2$ and FeO$_2$He are obtained by the empirical formula based on the elastic constant (Fine et al., 1984), and the relationship between the melting point and the elastic constant for the cubic system is $T_m = [553K + (5.91K/GPa)c_{11}] \pm 300K$. Geotherm data for the normal mantle and cold slab are derived from Litasov and Ohtani (2002) and Duan et al. (2018). The stable boundary data of pyrite type FeO$_2$ are derived from Zhang et al. (2017).
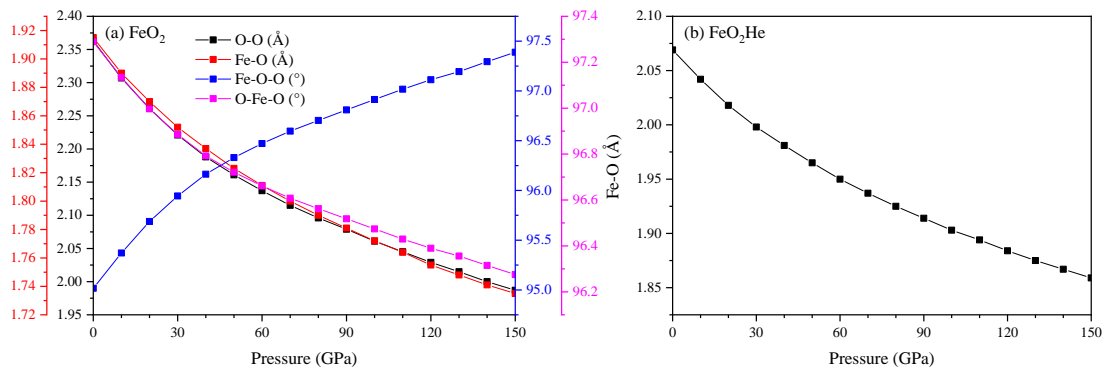

Fig. S4. Bond length and bond angle of (a) FeO$_2$ and (b) FeO$_2$He at different pressures.
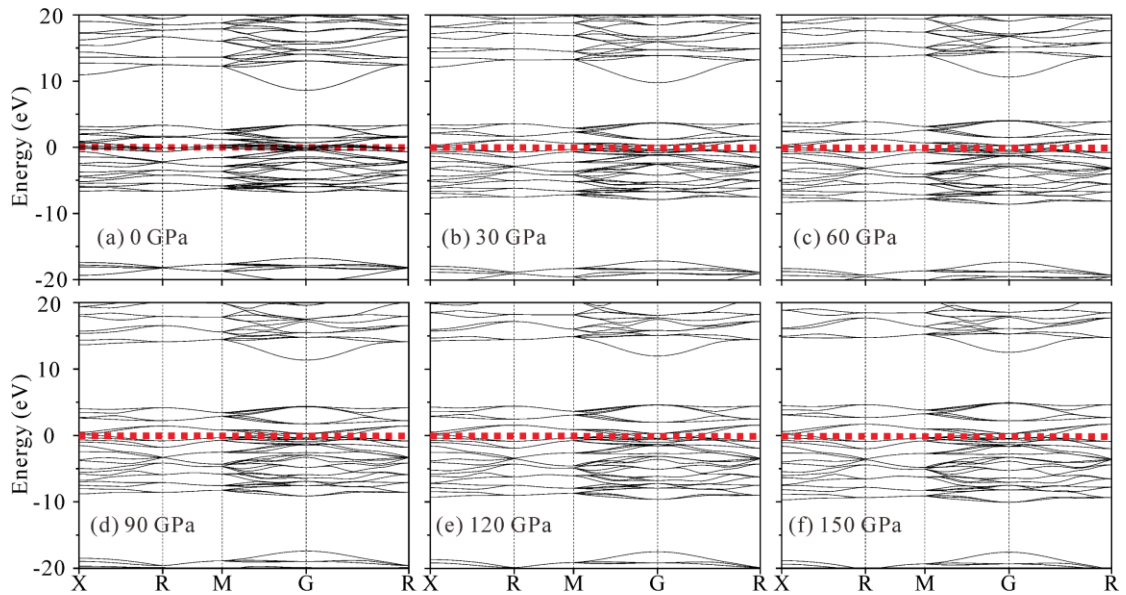

Fig. S5. Energy band structure of FeO$_2$ at different pressures. The red horizontal dashed line represents the Fermi level position (level = 0 eV).
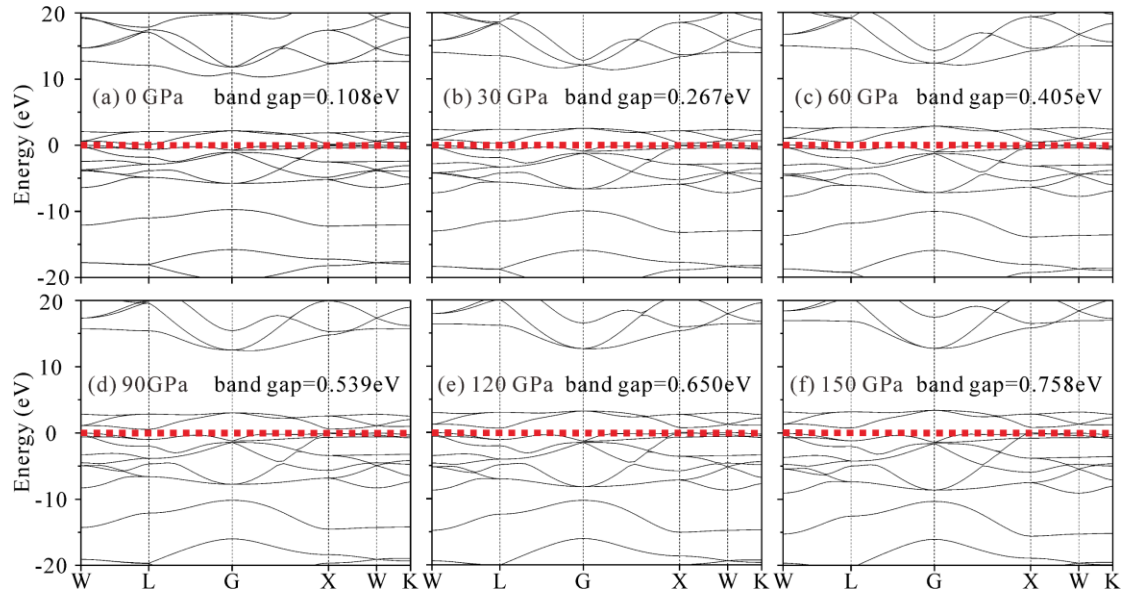
Fig. S6. Energy band structure of FeO$_2$He at different pressures. The red horizontal dashed line represents the Fermi level position (level = 0 eV).
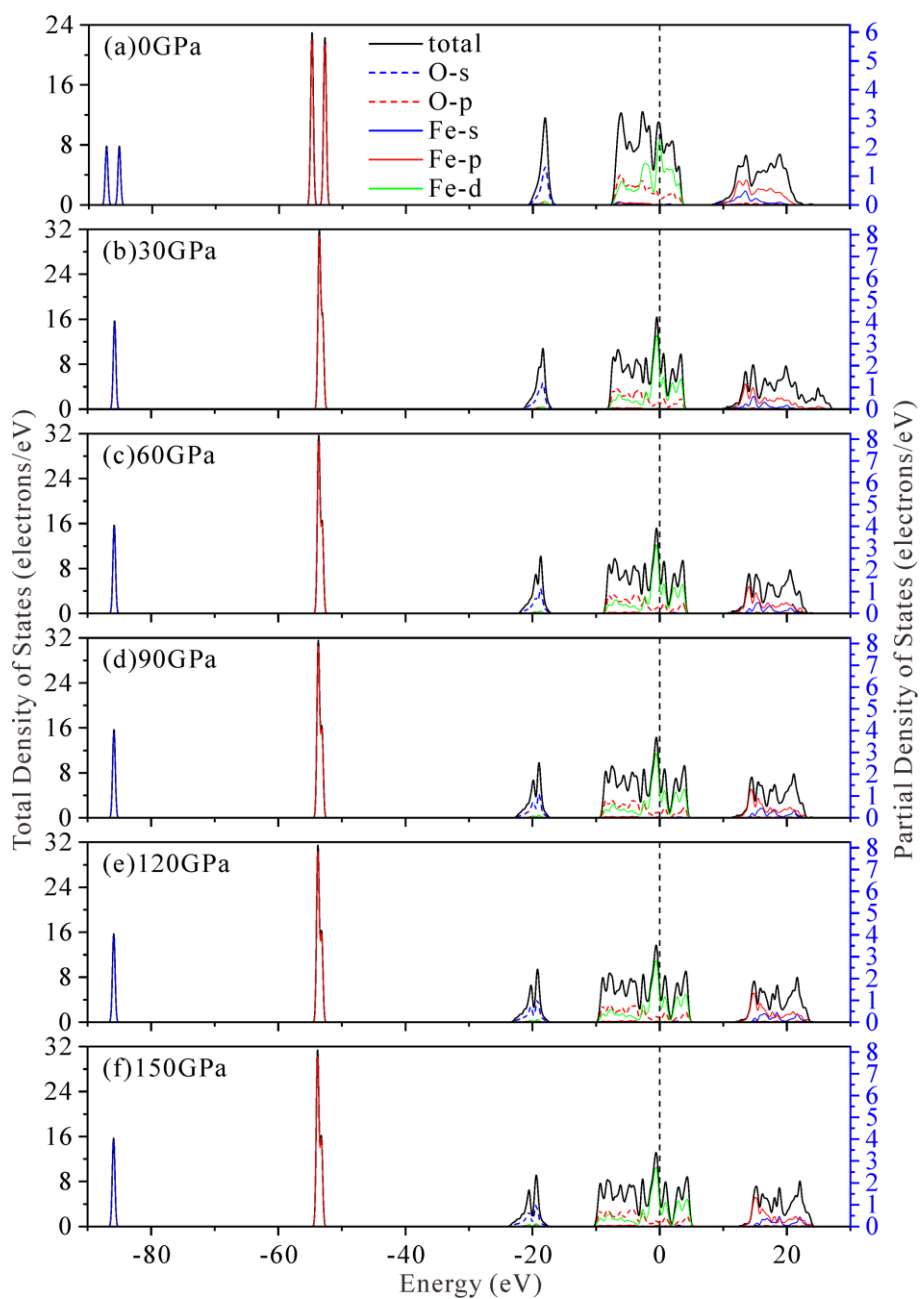
Fig. S7. Density of states of FeO_2 at different pressures. The black vertical dotted line represents the Fermi level position (level = 0 eV). The double peaks at -90–-80 eV and -60–-50 eV at 0 GPa are generated by spin-up and spin-down electrons, respectively.
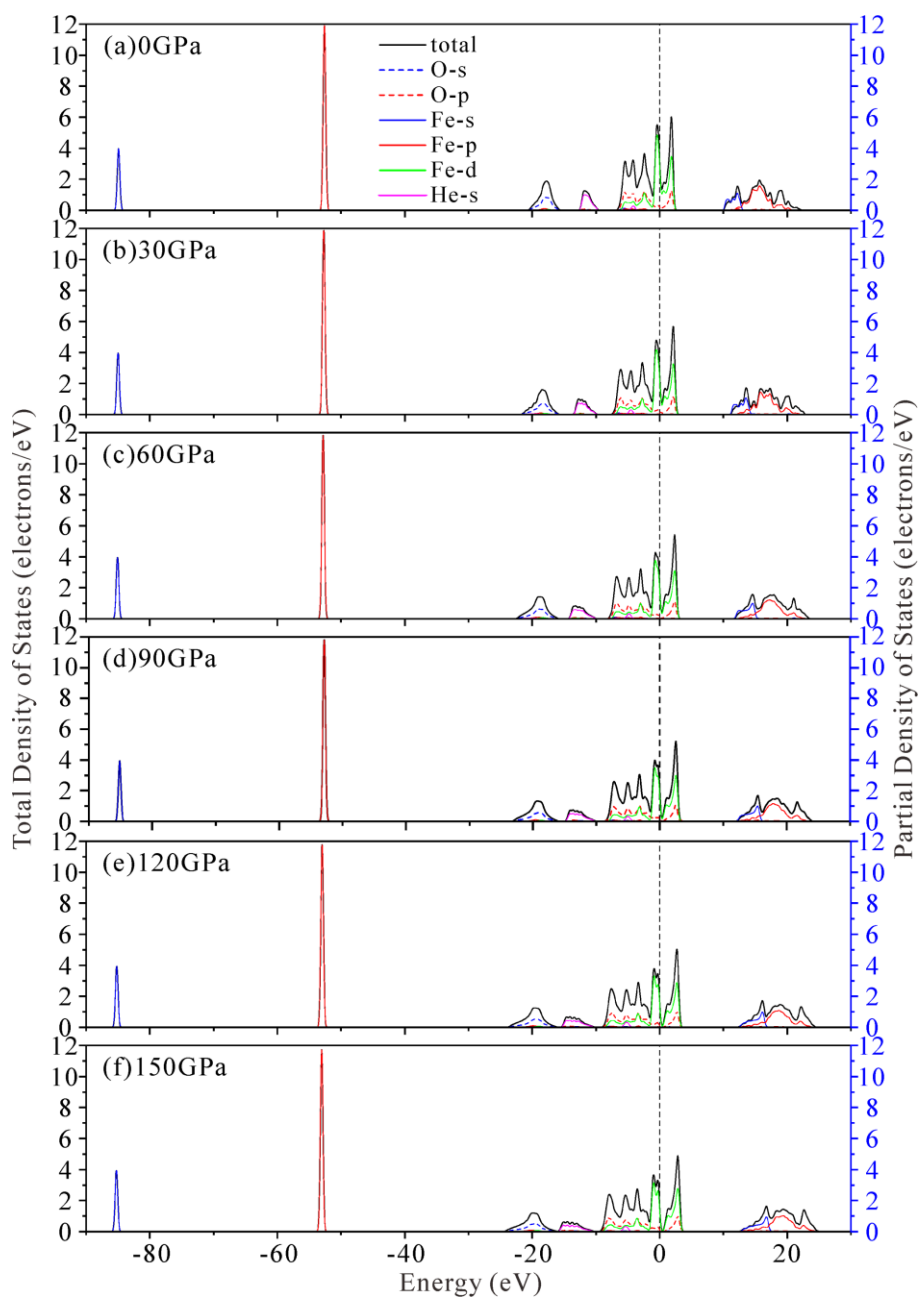
Fig. S8. Density of states of FeO_2He at different pressures. The black vertical dotted line represents the Fermi level position (level = 0 eV).
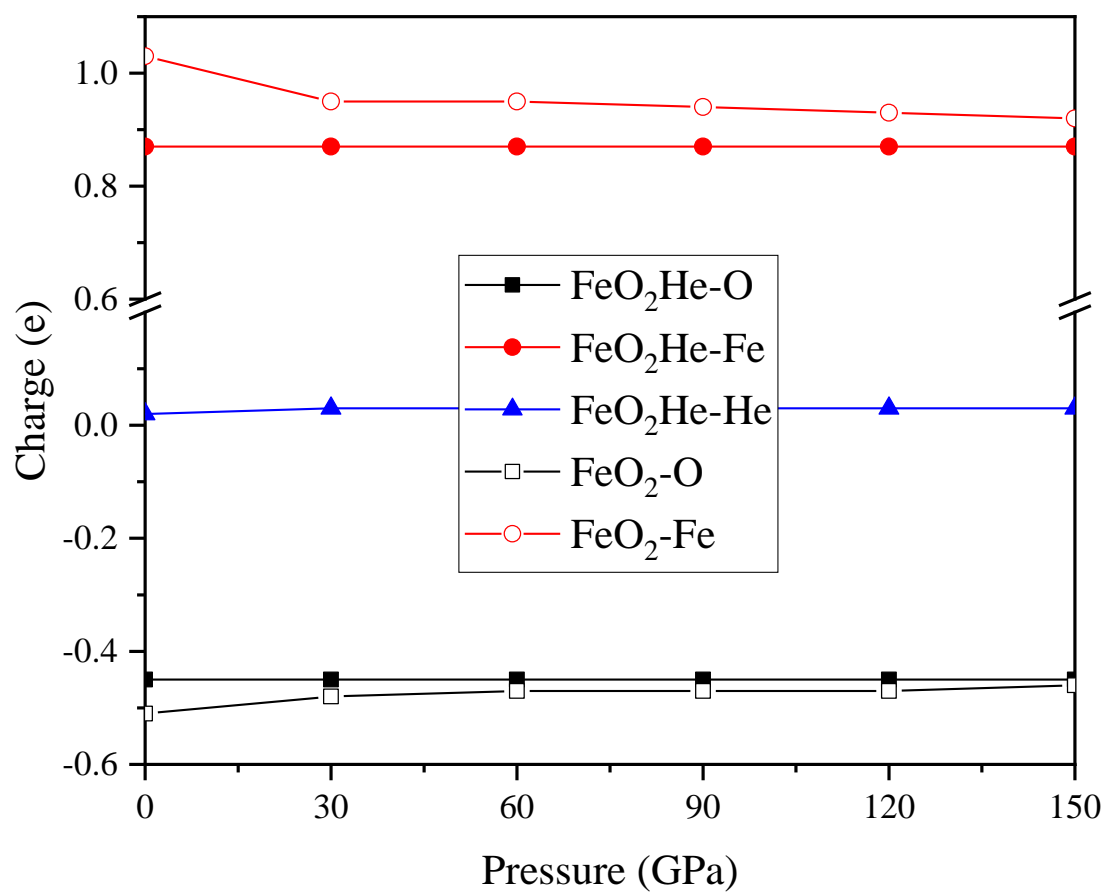
Fig. S9. Population analysis of FeO_2 and FeO_2He at different pressures. A positive value represents the loss of electrons and a negative value represents the gain of electrons.
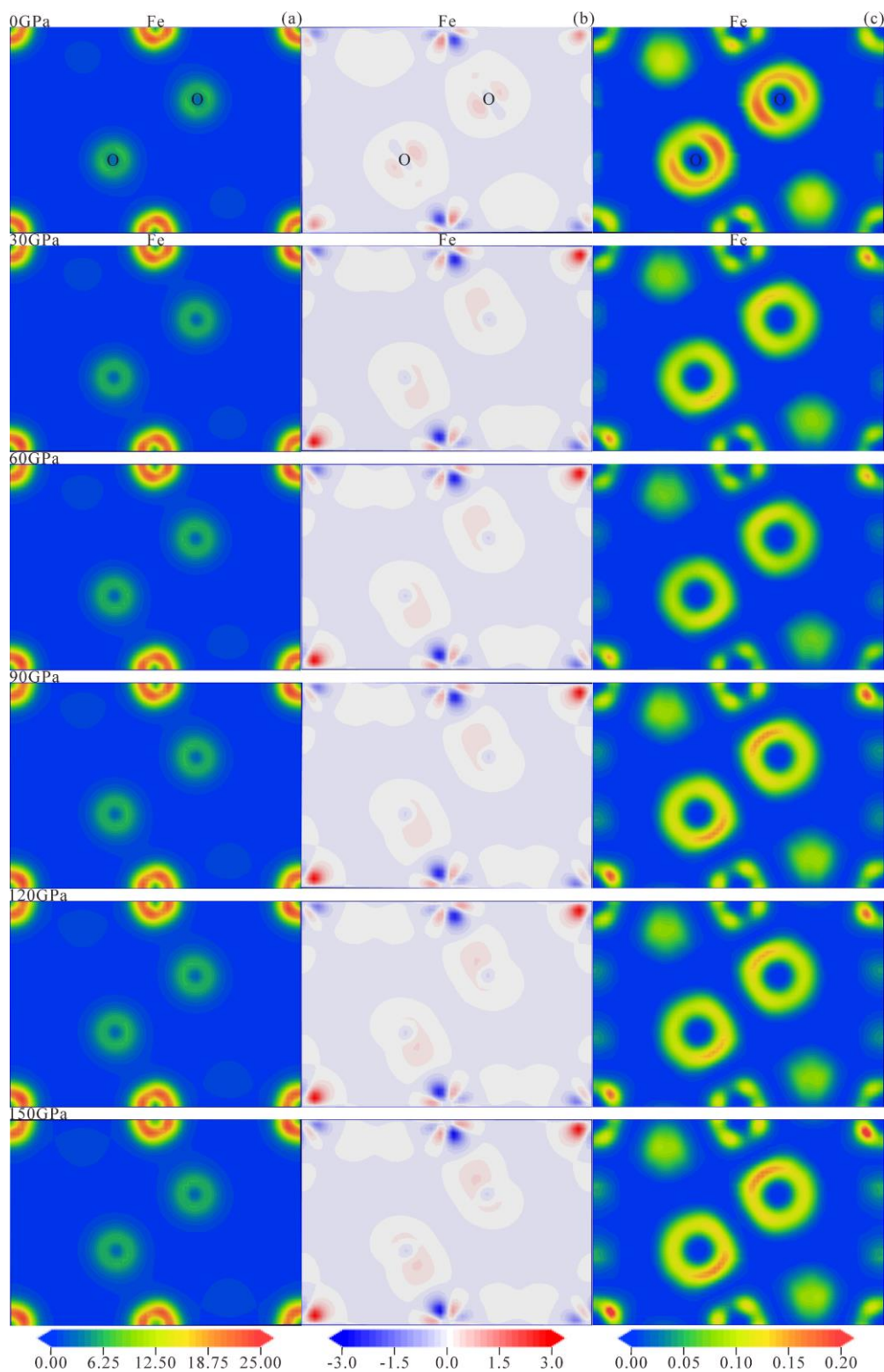
Fig. S10. (a) Electron density (left), (b) electron density difference (middle) and (c) electronic local function (right) of FeO_2 at different pressures. The red represents getting electrons and the blue represents losing electrons in the electron density difference.

Fig. S11. (a) Electron density (left), (b) electron density difference (middle) and (c) electronic local function (right) of FeO_2He at different pressures. The red represents getting electrons and the blue represents losing electrons in the electron density difference.
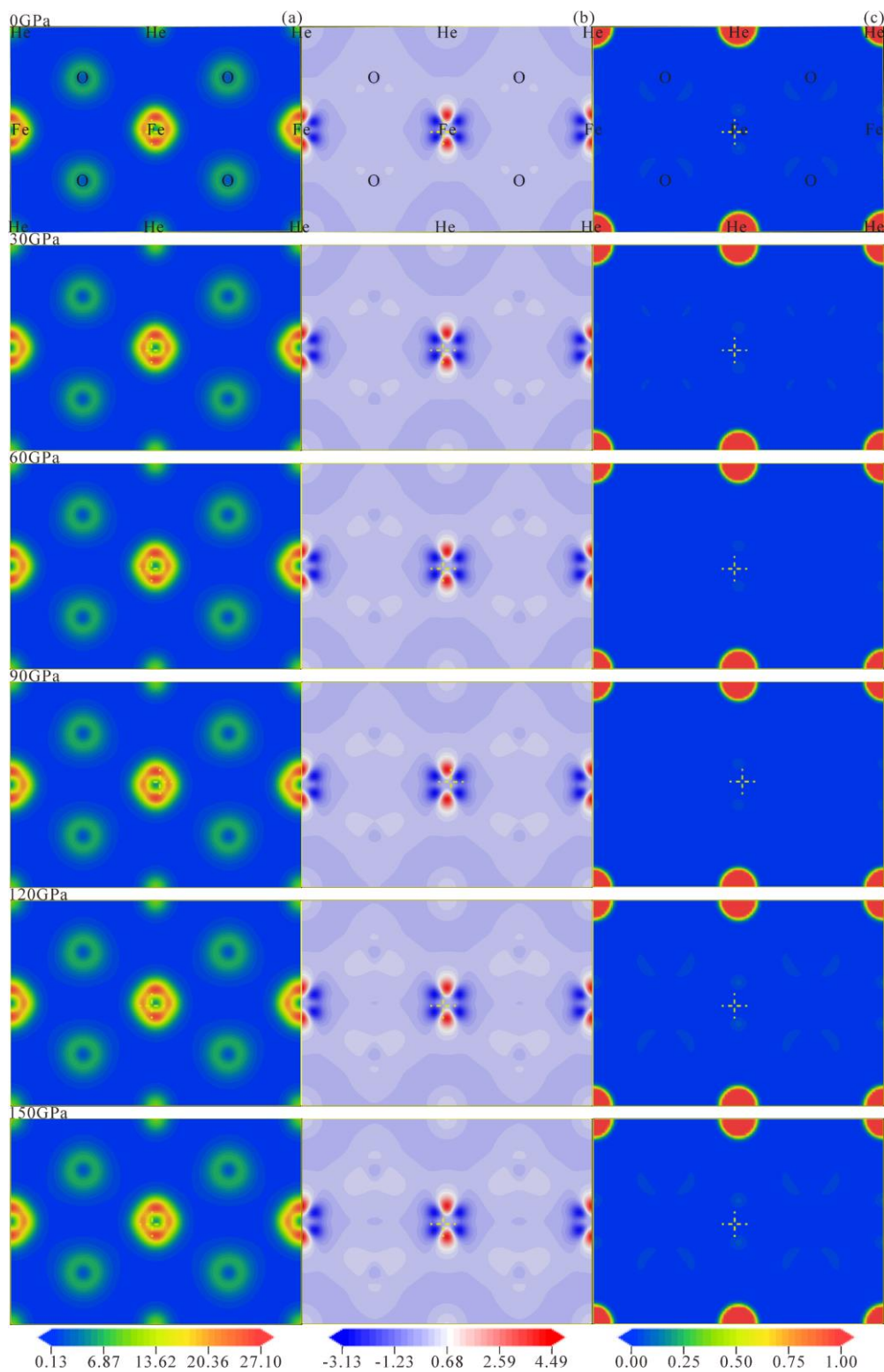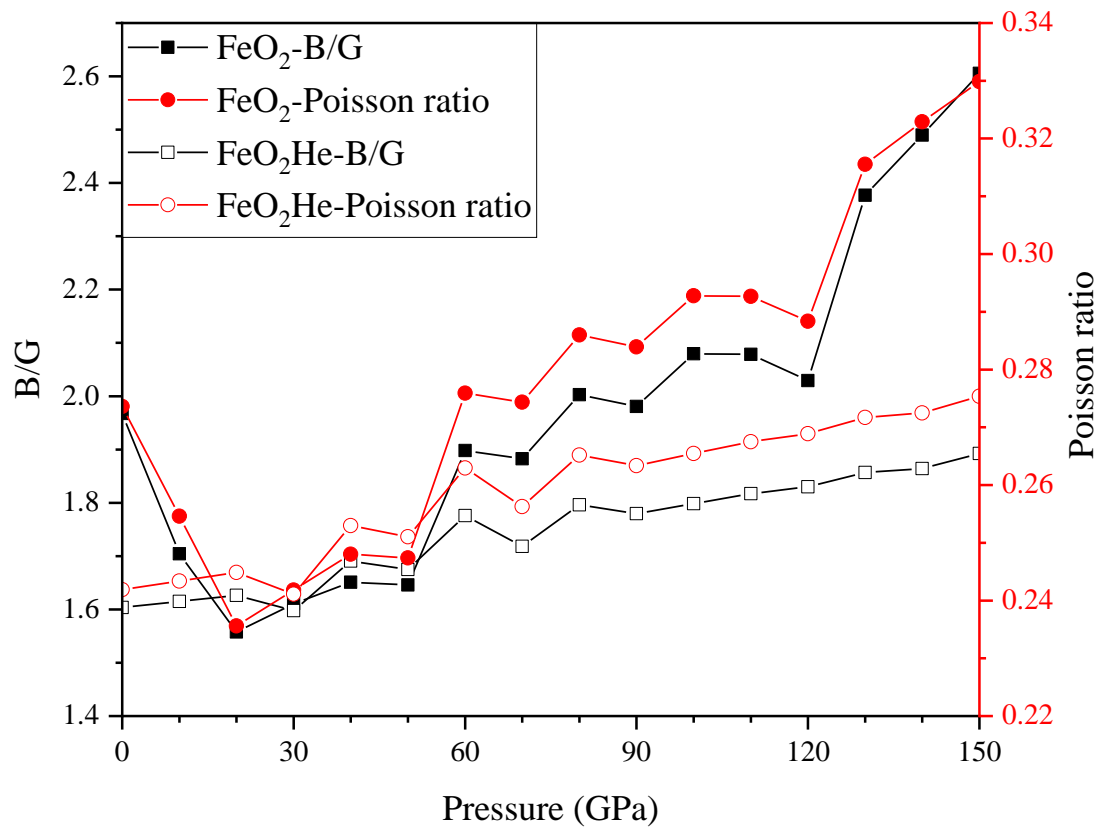
Fig. S12. Poisson's ratio and Pugh ratio of FeO_2 and FeO_2He at different pressures.

References

Duan, Y., Sun, N., Wang, S., Li, X., Guo, X., Ni, H., Prakapenka, V.B., Mao, Z., 2018. Phase stability and thermal equation of state of δ-AlOOH: Implication for water transportation to the Deep Lower Mantle. Earth Planet. Sci. Lett. 494, 92-98.

Fine, M.E., Brown, L.D., Marcus, H.L., 1984. Elastic constants versus melting temperature in metals. Scr. Metall. 18, 951-956.

Hu, Q., Kim, D.Y., Yang, W., Yang, L., Meng, Y., Zhang, L., Mao, H.K., 2016. FeO_2 and FeOOH under deep lower-mantle conditions and Earth's oxygen-hydrogen cycles. Nature 534, 241-244.

Jang, B.G., Kim, D.Y., Shim, J.H., 2017. Metal-insulator transition and the role of electron correlation in FeO_2. Phys. Rev. B 95, 075144.

Litasov, K., Ohtani, E., 2002. Phase relations and melt compositions in CMAS–pyrolite–H_2O system up to 25 GPa. Phys. Earth Planet. Inter. 134, 105-127.

Lu, C., Amsler, M., Chen, C., 2018. Unraveling the structure and bonding evolution of the newly discovered iron oxide FeO_2. Phys. Rev. B 98, 054102.

Shorikov, A.O., Poteryaev, A.I., Anisimov, V.I., Streltsov, S.V., 2018. Hydrogenation-driven formation of local magnetic moments in FeO_2H_x. Phys. Rev. B 98, 165145.

Zhang, J., Lv, J., Li, H., Feng, X., Lu, C., Redfern, S.A.T., Liu, H., Chen, C., Ma, Y., 2018. Rare helium-bearing compound FeO_2He stabilized at deep-Earth conditions. Phys. Rev. Lett. 121, 255703.

Zhang, X.L., Niu, Z.W., Tang, M., Zhao, J.Z., Cai, L.C., 2017. First-principles thermoelasticity and stability of pyrite-type FeO_2 under high pressure and

temperature. J. Alloys Compd. 719, 42-46.